CHAPTER 4

CHAPTER 4

Friction and Wear Behaviour of Ti-TiB-Fe Composites

This chapter begins with the presentation of results pertaining to the characterization of TiBFe composites fabricated via spark plasma sintering having either fixed content of B or Fe. This is followed by the results on reciprocating friction and wear behavior of these composites under different normal loads of 10, 15, 20, and 25 N and a constant frequency of 5 Hz, which are presented in two parts based on composition (a) Ti-TiB-Fe composites with varying amount of Fe at a fixed content of B and (b) Ti-TiB-Fe composites with varying boron and a fixed amount of Fe. The observed behaviour has been discussed in light of features observed after the SEM and XRD examination of worn surfaces and wear debris, to develop a coherent understanding on the correlation of composition and tribological behavior of composites and to explore the operative mechanisms of wear.

4.1 RESULTS: Ti-TiB-Fe COMPOSITES WITH VARRYING AMOUNT OF Fe

4.1.1 CHARACTERIZATION OF COMPOSITES

Figure 4.1 (a through c) shows the X-ray diffraction patterns of composites synthesized in the present study, whereas Table 1 presents the hardness and density of

respective composites. All the diffraction patterns show the peaks corresponding to the presence of TiB and β-Ti, as evident from Fig. 4.1, confirming thus the occurrence of reaction between raw Ti and TiB_2 to produce in situ TiB. No peaks corresponding to TiB_2 could be seen in X-ray diffraction pattern, indicating that whole TiB_2 was consumed during reaction leading to formation of TiB. Peaks showing the presence of intermetallic FeTi could also be observed in the diffraction pattern of composites, TiBFe1020 and TiBFe1030, containing 20 and 30 at.% Fe, respectively, as seen in Fig. 4.1 (b) and (c). The intensity of peaks corresponding to FeTi is observed to increase with an increasing amount of Fe, which is clear from a comparison of Fig. 4.1 (b) and (c). However, no peak for FeTi could be detected for composite TiBFe1010 containing 10 at.% Fe as evident from Fig. 4.1 (a), either it may not have been formed or amount of FeTi might have been below the detection limit of the diffractometer.

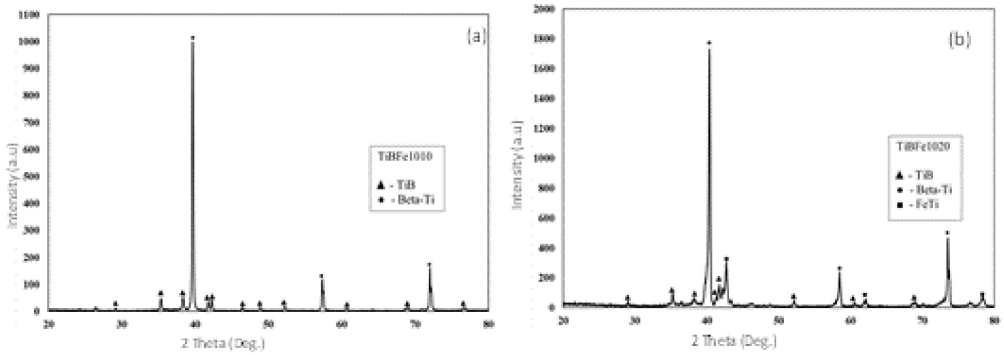

Figure 4. 1 XRD pattern of as prepared composites (a) TiBFe1010 (b) TiBFe1020 (c), and TiBFe1030

Figure 4.2 presents the SEM images illustrating the microstructure of different composites. One may observe the presence of light and dark gray phases along with some white phase in all the micrographs. Light gray areas correspond to the β-Ti, whereas the dark gray regions are TiB phase, which is developed in situ by reaction between Ti and TiB_2, and the presence of these are confirmed by the XRD shown in Fig. 4.1. The white phase is FeTi, as shown by the arrow in the micrograph. The content of FeTi increases with increasing Fe content, which is reflected by the increased presence of FeTi in microstructure as evident from a comparison of Figs. 4.2 (a through f). Elemental mapping helps in identifying the phases. For example, in the case of iron, the highest content of iron is expected in the FeTi phase, followed by β-Ti and TiB phases. Similarly, the highest amount of Ti is expected from the locations where β-Ti is present in comparison with areas of FeTi and TiB phases. A higher amount of boron is present in the regions of TiB phases compared to other areas. All this information were combined along with their morphologies to identify phases. The same has also been revealed by XRD, which have high peaks representing the presence of FeTi. Fe-Ti phase diagram reveals that solid solubility limit of Fe in β-Ti phase in about 15 at.%; hence, the presence of FeTi is observed in composites

containing 20 and 30 at.% Fe. Additionally, it may also be seen from these micrographs that size of dark gray areas, i.e., TiB, decreases and becomes finer with increasing content of Fe as one moves from Fig. 4.2 (a through c) reflecting thus, the role of Fe in refining TiB. Both the hardness and the density of composites are found to increase with an increasing amount of Fe in the composites, as seen from Table 4.1. An increase in hardness with an increasing amount of Fe (Table 4.1) may be attributed to the formation of FeTi, which is brittle and hard, and to the reduction in size of TiB, which acts as the barrier to the movement of dislocations.

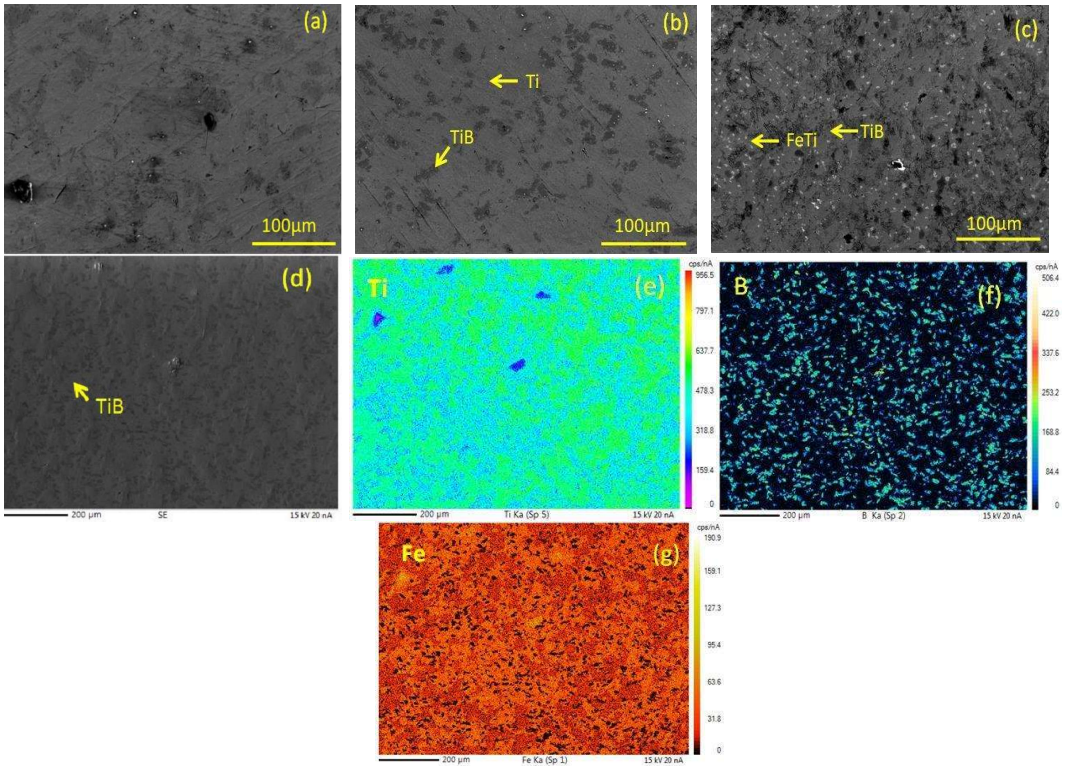

Figure 4. 2 Scanning electron micrographs showing the microstructure of composites (a) TiBFe1010, (b) TiBFe1020, and (c) TiBFe1030 (d) Micrograph of composite TiBFe 1030 used for colour mapping, and (e, f, g) show the presence Ti, B, and Fe, respectively

Table 4. 1 Designation porosity, hardness, and density of composites

Designation	**Porosity**	**Hardness** ($HV_{0.1}$)	**Density** (kg/m^3)

Ti-TiB_2-10 at. % Fe **(TiBFe1010)**	1± 0.3%	488±11	4.84
Ti-TiB_2-20 at. % Fe **(TiBFe1020)**	1 ± 0.7%	718±15	5.22
Ti-TiB_2-30 at. % Fe **(TiBFe1030)**	1 ± 1.0%	871±10	5.34

4.1.2 FRICTION AND WEAR BEHAVIOR OF COMPOSITES

(i) Variation of coefficient of friction with time

Figure 4.3 (a through d) depicts the typical variation of coefficient of friction (COF) with time at different loads for composites i.e., TiBFe1010, TiBFe1020, and TiBFe1030. One may observe that the coefficient of friction increases after the beginning of the test and then fluctuates around a mean level before being stabilized. The amplitude of fluctuation at 10 N is high for all composites and show a wavy trend during test duration. However, the amplitude of fluctuations is relatively less at 15 N for TiBFe1020, (stabilize after 200 seconds) in comparison to TiBFe1010 and 1030 with the waviness pattern (stabilize after aprox 400 sec). However, at the load 20 N, TiBFe1010 and TiBFe1020 composites (stabilize after approx 200 seconds) while TiBFe1030 show a stable fluctuation from the starting to the end of the test. At 25 N the fluctuation is seen to be high till 400 seconds for TiBFe1010, and TiBFe1030 before getting stabilize to a mean position while TiBFe1020 shows a high peak at approx 300 seconds before being stabilize at 400 seconds with a minimum fluctuation about mean position in comparison to the other composites.

(ii) Variation of average coefficient of friction with normal load and composition

Figure 4.4 (a) shows the variation of average coefficient of friction with load for all the composites, whereas Fig. 4.4 (b) illustrates the same with respect to the composition at

different loads. The coefficient of friction for composite TiBFe1010 shows a sharp increase in coefficient of friction with the load from 10 to 25 N as observed in Fig. 4.4 (a). In contrast, the coefficient of friction for TiBFe1020 decreases from 10 N to 15 N, and further marginally decreases is observed at 20 N before increasing sharply at 25 N whereas,TiBFe1030 reflects a decreasing tendency from 10 N to 20 N and further increases sharply at 25 N. The variation of the coefficient of friction with the composition shown in Fig. 4.4 (b) also reveals a decreasing tendency for all composites with an increasing amount of Fe. At 10 N, the decrease is marginal, while at 25 N the decrease of COF is sharp with the increase in Fe. Whereas, 15 N and 20 N show a decreasing trend of COF with increasing amounts of Fe, as evident from Fig. 4.4 (b).

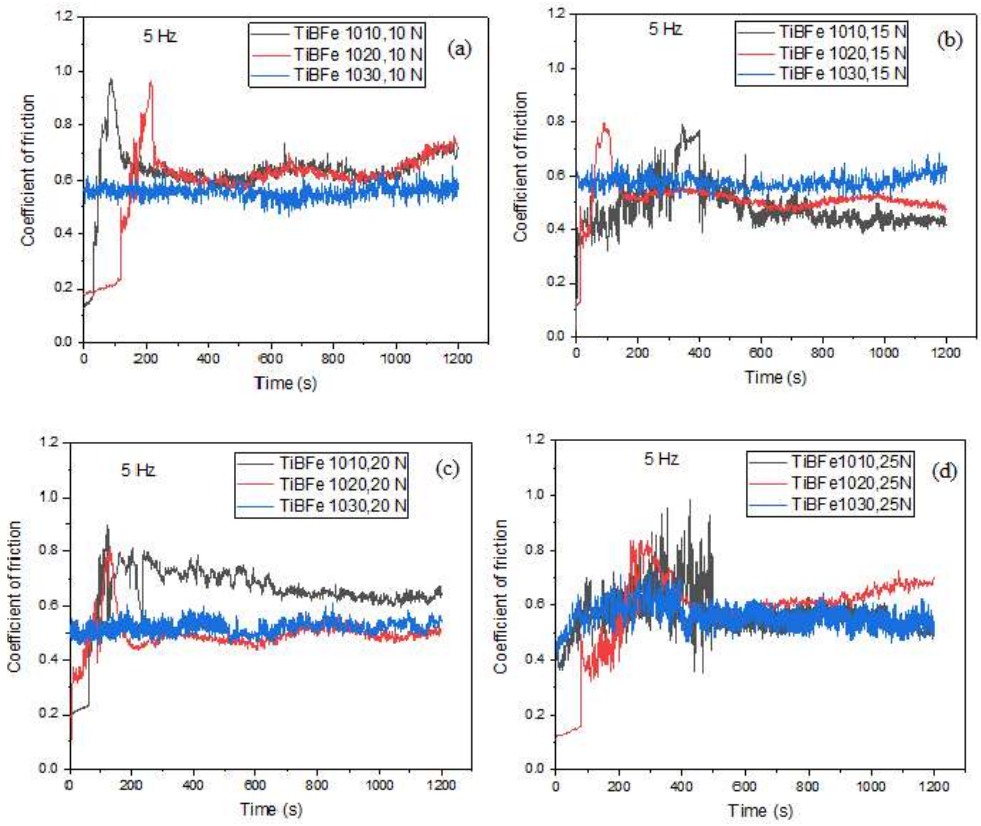

Figure 4. 3 Variation of coefficient of friction with time for TiBFe1010, TiBFe1020, and TiBFe1030 composites at different loads (a) 10 N, (b) 15 N, (c)20 N, and (d) 25 N

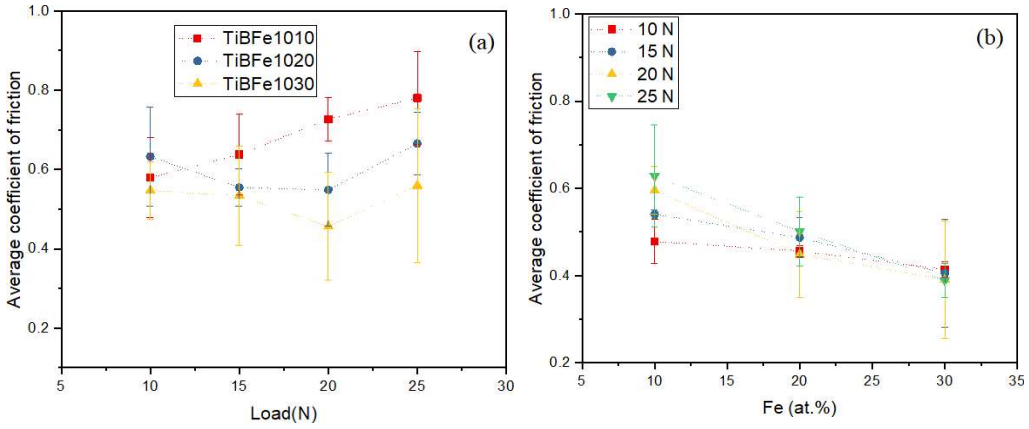

Figure 4. 4 Variation of average coefficient of friction (a) load and (b) composites Fe (at.%)

(iii) Variation of wear rate with normal load and composition

The variation of wear rate with load for all the composites shown in Fig. 4.5 (a) depicts no particular trend. The composite containing 10 at.% Fe, i.e., TiBFe1010, has the highest wear rate at all the loads, and the wear rate is observed to decrease sharply as the load is increased from 10 to 15 N followed by an increase till 20 N load before decreasing again beyond that as seen from Fig. 4.5 (a). The decrease in wear rate is observed for TiBFe1020 as the load is raised from 10 to 20 N before increasing marginally to 25 N, whereas for TiBFe1030 it has been observed to increase from 10 N to 20 N followed by a decrease till 25 N. One may also note that TiBFe1020 has the lowest wear rate at all the loads among all the composites. There is a sharp decrease in wear rate is observed as one moves from TiBFe1010 to TiBFe1020 followed by an increase for TiBFe1030 as evident from Fig. 4.5 (b) for all composites.

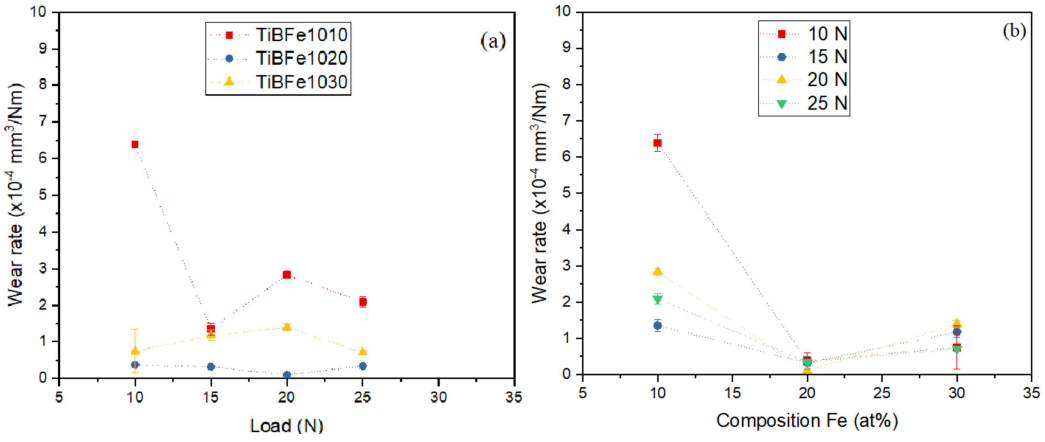

Figure 4. 5 Variation of wear rate of the composites TiBFe1010, TiBFe1020, and TiBFe1030 with (a) load and (b) composites Fe (at.%)

4.1.3 Examination of Worn Surface of Composites

SEM micrographs of the worn surfaces of TiBFe1010, TiBFe1020, and TiBFe1030 at loads of 10, 15, 20, and 25 N are presented in Figs. 4.6, 4.7, 4.8, and 4.9, respectively. Figure 4.6 (a through c) presents SEM images of the worn surfaces of TiBFe1010, TiBFe1020, TiBFe1030 composites, respectively, after sliding against the steel ball at the lowest of 10 N used in the present study. All the surfaces reveal the presence of wear grooves running parallel to sliding direction along with a transfer layer of wear debris (probably containing oxides also) with different degree of compaction and area of coverage on the worn surface despite having undergone the same level of frictional heating. A loosely bound and patchy transfer layer could be seen on the worn surface of TiBFe1010 (Fig. 4.6 a) along with some loose wear particles which may cause abrasion during sliding motion. However, the transfer layer is relatively more compact for TiBFe1020 and TiBFe1030 as evident from Fig. 4.6 (b) and (c) which is helpful in reducing the metal–metal contact at interface. The transfer layer also appears to have detached at some places due to tribo-stress as seen from the detached or delaminated regions in Fig. 4.6 (a through c). However, the layer is observed to be cracked and detached at more number of locations in TiBFe1030

than in TiBFe1020 as evident from a comparison with Figs. 4.6 (b) and (c) which might have caused relatively higher loss of material in TiBFe1030 than TiBFe1020 as observed in Fig. 4.6 (a).

Figures 4.7 (a through c) present the morphology of the worn surface of composites tested under a load of 15 N. The surface of TiBFe1010 worn at a load of 15 N, presented in Fig. 4.7 (a) reveals the presence of very few wear debris particles and a transfer layer along with some scoring marks. The worn surface of TiBFe1020 (Fig. 4.7 b) also shows the presence of a transfer layer but the extent of coverage is more in comparison to TiBFe1010. Fig. 4.7 (c) shows the presence of a very smooth and compacted tribo-layer on the worn surface of TiBFe1030 composite. However, the layer appears to have been detached at few places.

The morphologies of the surfaces of TiBFe1010, TiBFe1020, and TiBFe1030 worn at 20 N load are presented in Figs.4.8 (a through c). In Fig. 4.8 (a), the worn surface of TiBFe1010 composite appears to have fine wear debris particles containing elements of composite materials, whereas, it is found to be covered with a compacted and smooth tribo-layer with very few visible scoring marks at several locations for TiBFe1020 as seen from Fig. 4.8 (b). However, one could observe the existence of a very smooth and compacted tribo-layer (Fig. 4.8 c) of wear debris on the worn surface of TiBFe1030 composite.

Figure 4.9 (a through c) shows the morphologies of the surface of composites worn after sliding at a load of 25 N load. All surfaces are covered with a relatively smooth and well-compacted transfer layer of wear debris, due to which the wear tracks are visible only slightly except in Fig. 4.9 (c) for TiBFe1030, where relatively deeper grooves are visible along the sliding direction. However, this transfer layer is observed to have detached at different places which might have given rise to wear debris. The extent of cover provided

by the transfer layer and its level of compaction is more at the highest load of 25 N in comparison with the lowest load of 10 N used in the present study, which can be judged by a comparison of Fig. 4.6 (a through c) and 4.9 (a through c). Figure 4.6 (d) shows the SEM micrograph of the worn surface of TiBFe1010 after sliding at a load of 10 N along with the EDS analyses of different spots (1, 2, 3, and 4) marked on the micrograph. EDS analyses reveal the presence of high amount of oxygen on all spots (1through 4), indicating a possibility of oxidation of metallic elements at the surface. EDS analyses for other composites also revealed the similar results and hence not presented here to avoid repetition.

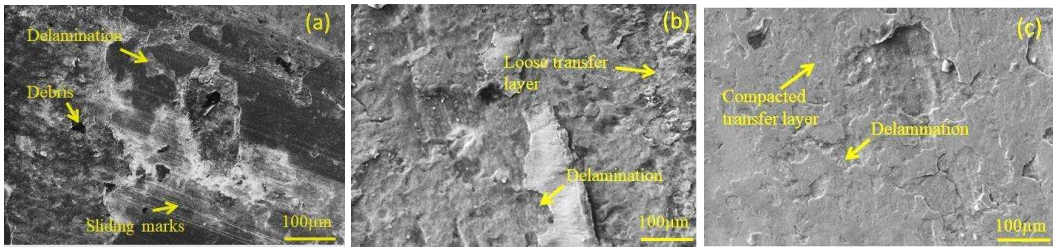

Figure 4. 6 SEM images of worn surfaces of composite at a load of 10 N (a) TiBFe1010 (b) TiBFe1020 and (c) TiBFe1030

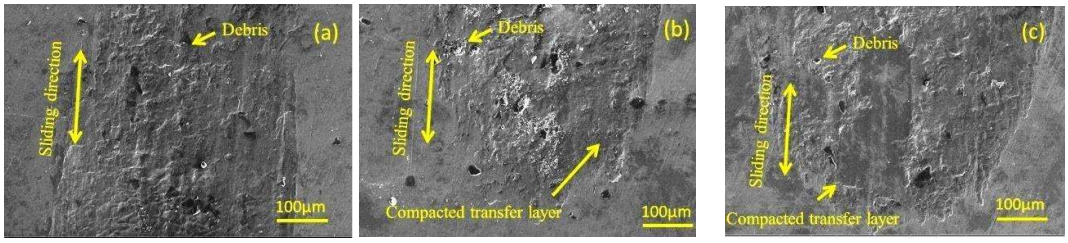

Figure 4. 7 SEM images of worn surfaces of composite at a load of 15 N (a) TiBFe1010 (b) TiBFe1020 and (c) TiBFe1030

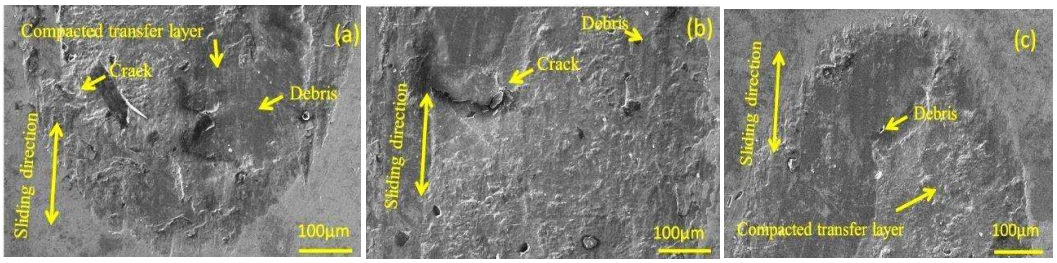

Figure 4. 8 SEM images of worn surfaces of composite at a load of 20 N (a) TiBFe1010 (b) TiBFe1020 and (c) TiBFe1030

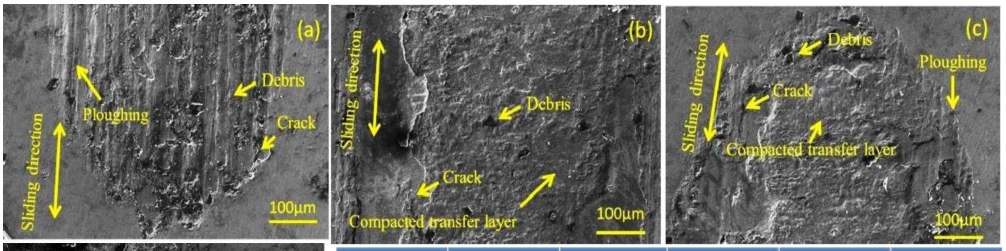

Spot No.	B K(at%)	C K(at%)	O K(at%)	Ti K(at%)	Fe K(at%)
1	23.26	25.25	27.54	1.85	21.40
2	21.97	17.84	38.13	1.55	20.52
3	13.18	5.80	41.39	1.87	37.75
4	15.06	10.86	44.19	10.57	19.33

Figure 4. 9 SEM images of worn surfaces of composite at a load of 25 N (a) TiBFe1010 (b) TiBFe1020 (c) TiBFe1030 and (d) EDS of TiBFe1030

4.1.4 Worn Surface Morphology of Counterface

The morphologies of the worn surface of the bearing steel ball slid against TiBFe1010, TiBFe1020, and TiBFe1030 composites at loads of 10, 15, 20, and 25 N are presented in Figs. 4.10, 4.11, 4.12, and 4.13, respectively**.** The morphology of the bearing steel ball slid against TiBFe1010 at a load of 10 N and depicted in Fig. 4.10 (a) reveals the presence of a layer of transferred material from the composite at the bottom left corner along with a rough region from where the transferred material appears to have been detached during the sliding motion. The worn surface of the ball slid against TiBFe1020 illustrated in Fig. 4.10 (b) shows a smooth surface with a layer of compacted material

transferred from the composite along the direction of sliding. The worn surface of bearing steel ball slid against TiBFe1030 composite given in Fig. 4.10 (c) also reflects the presence of a tribo- layer of transferred material from the composite to the bearing steel ball but the layer does not appear to be well compacted at several locations.

The worn surface of the bearing steel ball slid against TiBFe1010 composite at a load of 15 N also shows a compacted and relatively smooth layer in some places along with the presence of some transferred material from the composite as seen in Fig. 4.11 (a). However, the detachment of layer is also observed on the surface. Fig. 4.11 (b) shows the presence of a relatively well-compacted and continuous transfer layer of TiBFe1030 composite. The worn surface of the bearing steel ball slid against TiBFe1030 composite given in Fig. 4.11 (c) also reflects the presence of a tribo-layer.

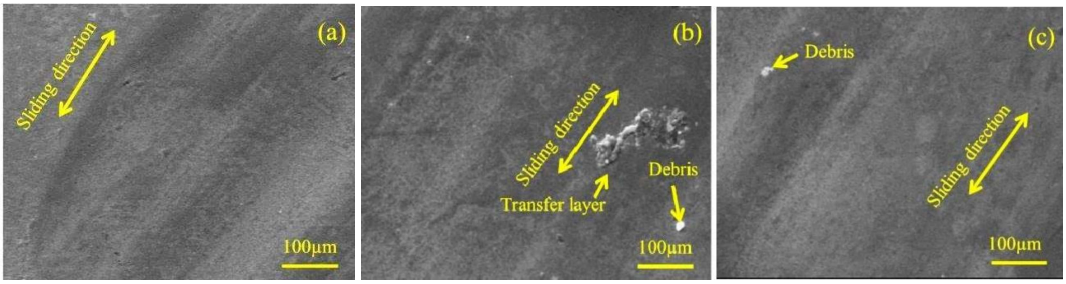

Figure 4. 10 Worn surfaces of bearing steel ball slid against (a) TiBFe1010 (b) TiBFe1020 (c) TiBFe1030 composite at a load of 10N

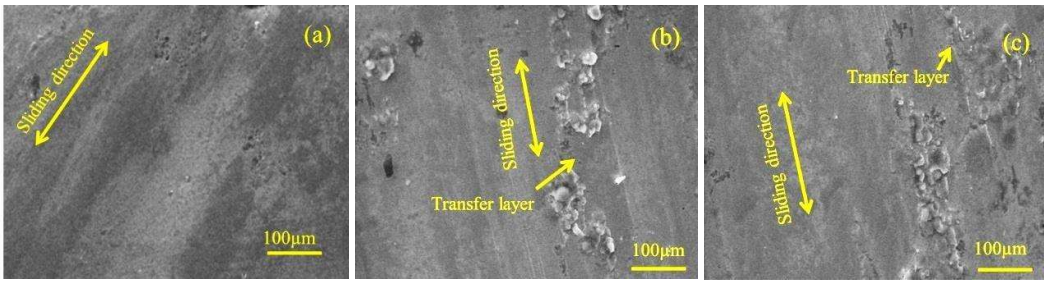

Figure 4. 11 Worn surfaces of bearing steel ball slid against (a) TiBFe1010 (b)

TiBFe1020 (c) TiBFe1030 composite at a load of 15N

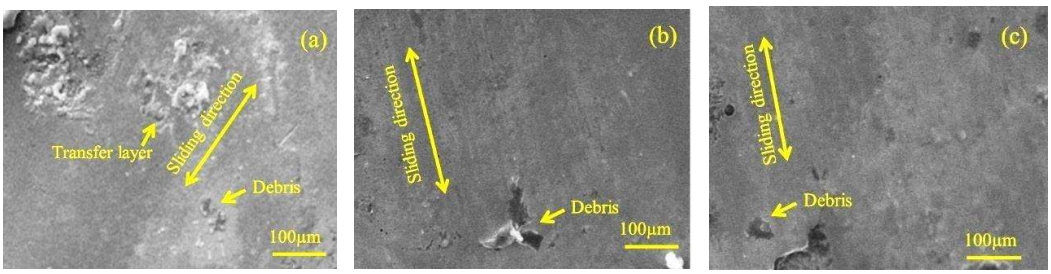

Figure 4. 12 Worn surfaces of bearing steel ball slid against (a) TiBFe1010 (b) TiBFe1020 (c) TiBFe1030 composite at a load of 20N

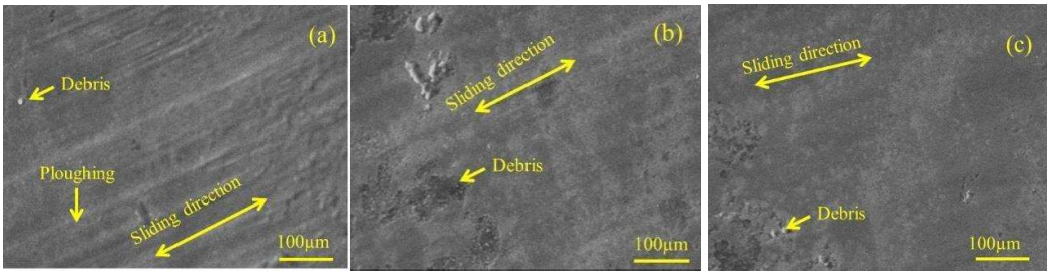

Figure 4. 13 Worn surfaces of bearing steel ball slid against (a) TiBFe1010 (b) TiBFe1020 (c) TiBFe1030 composite at a load of 25N

Figure 4.12 (a through c) illustrates the SEM micrographs of the worn surface of counterface ball slid against TiBFe1010, TiBFe1020, TiBFe1020 composites at a load of 20 N along with corresponding EDS spectra. The morphology depicted in Fig. 4.12 (a) presents a rough surface and the presence of transferred material from the TiBFe1010 to the steel ball. The worn surfaces of ball slid against TiBFe1020 and TiBFe1030 given in Figs. 4.12 (b) and (c), respectively, show the presence of a discontinuous transfer layer. The worn surface of steel ball slid against TiBFe1010 at the highest load of 25 N used in the present study is presented in Fig. 4.13. The surface reveals the presence of a well-compacted transfer layer, but the layer is found to have detached at some locations. The worn surface of the counterface ball slid against TiBFe1020 shows the presence of a well-

compacted and continuous transfer layer of transferred material from composite as seen in Fig. 4.13 (b). The worn surface of the bearing steel ball slid against TiBFe1030 composite given in Fig. 4.13 (c) also reflects the presence of a discontinuous layer of transferred material from composite which appears to have broken or detached at a few locations.

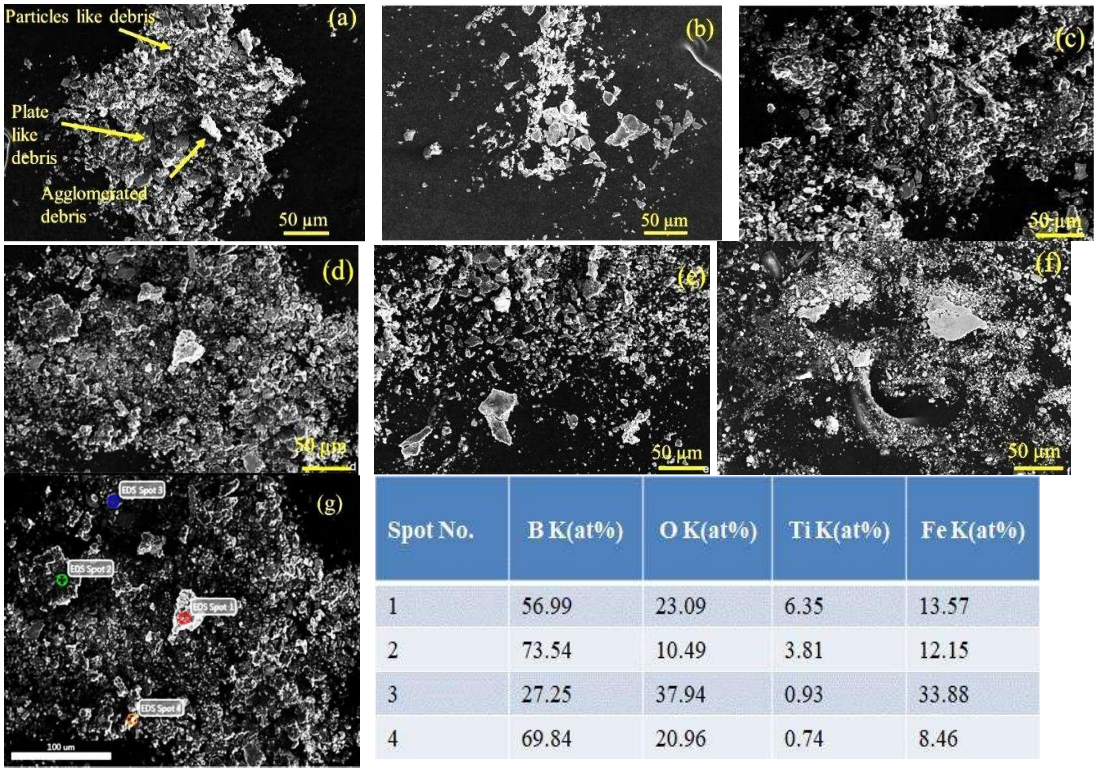

Spot No.	B K(at%)	O K(at%)	Ti K(at%)	Fe K(at%)
1	56.99	23.09	6.35	13.57
2	73.54	10.49	3.81	12.15
3	27.25	37.94	0.93	33.88
4	69.84	20.96	0.74	8.46

Figure 4. 14 SEM micrographs of wear debris (a) TiBFe1010 at 10N (b) TiBFe1020 at10N (c) TiBFe1030 at 10N (d) TiBFe1010 at 25N (e) TiBFe1020 at 25N(f) TiBFe1030 at 25N (g) EDS analysis of grey and white spots of Fig.8(d)

4.1.5 Examination of Wear Debris

Figure 4.14 (a through g) presents the morphologies of wear debris of different composites collected after sliding under the loads of 10 and 25 N, respectively, as examined under SEM. The debris is observed to be composed of some fine particles and some irregular shaped plate-like particles of different sizes along with some sheet type laminates, which may be the parts of the compacted transfer layer detached (Fig. 4.6 and 4.9) from

the surface during sliding. EDS analyses of the different locations of wear debris (marked in Fig. 4.14 g) presented in Table given besides Fig. 4.14 (g) reveal the presence of Fe, Ti, B, and oxygen with varying intensities indicating that either these were in elemental form or in the form of oxides of Ti and Fe. Since, the amount of debris collected for each composite was small, all the debris material was mixed together and subjected to x-ray diffraction analysis. Fig. 4.15 shows the XRD pattern of the collected wear debris, which reveals the presence of peaks corresponding βTi, FeTi, TiB, TiO_2, and Fe_2O_3 which have been identified using JCPDS files.

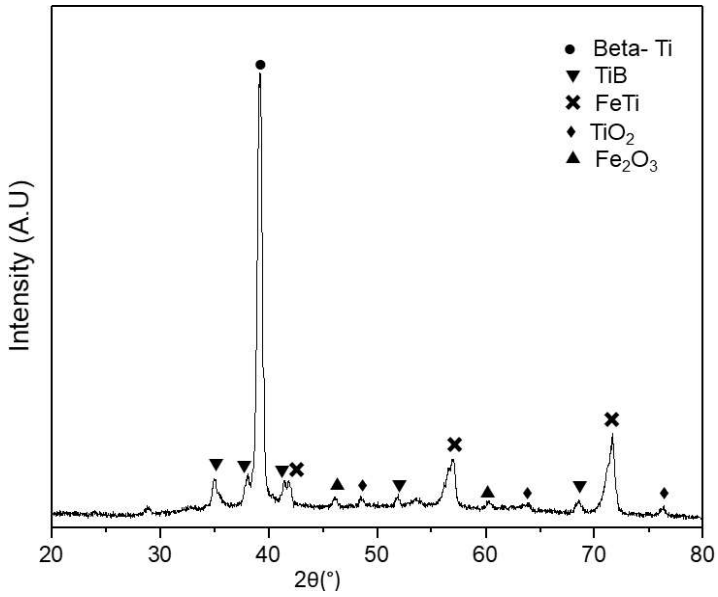

Figure 4. 15 XRD pattern of the wear debris collected after the wear tests

4.2 DISCUSSION

A relatively higher coefficient of friction observed for TiBFe1010 in comparison with other composites may be attributed to its relatively lower hardness compared to TiBFe1020 and TiBFe1030, resulting in a relatively higher real area of contact. The lowest friction shown by TiBFe1030 at all the loads shown in Fig. 4.4 may also be explained based

on its highest hardness leading to a relatively lower real area of contact. The other factor contributing to a lower friction coefficient may be the extent of cover provided by the transfer layer of wear debris containing TiO_2 and Fe_2O_3 as indicated by the EDS spectrum and XRD of wear debris given in Figs. 4.9, 4.14, and 4.15, respectively, which provides low shearing junctions at the interface and help in smooth sliding of bodies on relative motion, which causes abrasive wear. The presence of TiO_2 has been shown too beneficial in enhancing the wear resistance of coatings [89]. The worn surface of TiBFe1030 is observed to be covered by a smooth and relatively thick transfer layer, as evidenced from Figs. 4.6 (c), 4.7(c), 4.8 (c), and 4.9 (c). It has earlier been indicated that a substrate of higher hardness can retain a thicker transfer layer in comparison with a substrate of lower hardness before being detached due to interfacial stress. Hence, it is not surprising that the composite TiBFe1030 having the largest hardness among the composites investigated in the study has a relatively thicker transfer layer present on its surface. At a particular load, the friction coefficient has also been observed to decrease with increasing content of Fe, as seen from Fig. 4.4 (b), and the same may also be explained based on the presence of the transfer and its extent of coverage provided to the underlying substrate along which is helpful in reducing the metal–metal contact and, in turn, adhesion between the surfaces in contact.

Wear rate calculated as volume loss per unit distance of sliding has been observed to be the highest for TiBFe1010 and the lowest for TiBFe1020 with that of TiBFe1030 falling in-between at all the loads as seen from Fig. 4.5 (a). It is generally claimed that the wear rate is inversely proportional to the hardness of the material; hence, it is not surprising that it has been TiBFe1010, which is the least hard of the three composites has shown the highest rate of wear at all the loads. However, it is not only the hardness that affects the wear rate but also other wear phenomena occurring during sliding also play a decisive role

in controlling the friction and wear behavior. This is also evident from the observed higher wear rate of TiBFe1030 in comparison with TiBFe1020 despite former one being harder. The observed behavior may be explained based on the extent and compaction of the transfer layer present on the worn surfaces shown in Figs. 4.6, 4.7, 4.8 and 4.9. The worn surface of TiBFe1010 at 10 N presents a relatively torn surface (Fig. 4.6a), whereas, at 25 N, it reveals the presence of a compacted transfer layer that is seen to be detached at several places. This might have led to increased loss of material, and hence, a higher rate of wear from TiBFe1010. However, the surfaces of both TiBFe1020 and TiBFe1030 are covered by a smooth transfer layer both at 10 N and 25 N Fig. 4.6 (b and c)) and 4.9 (band (c). However, the worn surface of the TiBFe1030 shows some delamination [91] of the layer at the load of 10 N. In contrast, deep grooves running parallel to sliding direction are found to be present at 25 N, which might have increased its wear rate compared to TiBFe1020. The presence of grooves may be ascribed to the abrasive action of hard FeTi. The presence of FeTi in wear debris is confirmed by XRD shown in Fig. 4.14. The increasing amount of FeTi appears to be detrimental to the friction and wear properties despite improving the hardness due to its inherent brittleness. Hence, in the present study, TiBFe1020 containing a relatively lesser amount of FeTi (sufficient enough to impart hardness) is found to be the one having optimum mechanical and tribological characteristics under the conditions of testing used in the current study.

Based on the results and discussion presented above it can be inferred that Ti-based composites having a fixed amount of 13 wt.% TiB and a varying amount of Fe could be successfully synthesized through an in-situ reaction between Ti, Fe, and TiB_2. Iron (Fe) was added in 10, 20, and 30 at.% to find the optimum amount necessary to stabilize β-Ti. However, it resulted in the formation of intermetallic phase FeTi, which increased the hardness of the comstabilizedposite but had an adverse effect on tribological performance.

The coefficient of friction has been obsrved to show a decreasing tendency with increasing amount of Fe at each load and the composite containing 30 at. % Fe i.e., TiBFe1030 showed the lowest coefficient of friction. However, the lowest wear rate has been observed for TiBFe1020 having 20 at. % Fe despite its lower hardness than TiBFe1030 due to the dominating effect of transfer layer, its area coverage over the surface and detachment. The study has revealed the potential of Ti-TiB composites as a future tribo-material for sliding wear applications. The dominating mechanisms of wear have been found to be ploughing, abrasive, oxidation, and delamination.

4.3 RESULTS: Ti-TiB-Fe COMPOSITES WITH VARRYING AMOUNT OF B

4.3.1 CHARACTERIZATION OF COMPOSITES

The X-ray diffraction patterns of composites are shown in Fig. 4.16, whereas, Table 4.2 displays the designation, porosity, hardness, and density of the respective composites. Porosity refers to the density of the composites as how dense the composite is synthesized. More dense composites mean a high hardness value which ultimately improves the tribological properties of the composites. As shown in Fig. 4.16, all of the diffraction patterns show peaks corresponding to the presence of TiB and β-Ti, confirming the presence of a reaction between raw Ti and TiB_2 to produce in situ TiB. No peaks corresponding to FeTi is observed in TiBFe1010 and TiBFe2010, as shown by a comparison of Fig. 4.16(a and b). The spectrum of composite TiBFe3010 containing 30% B has fewer FeTi peaks as shown in Fig. 4.16(c). The amount of FeTi produced maybe less than the diffractometer's detection limit. The density and hardness of composites have been

observed to increase with increasing content of TiB as evident from Table 4.2. The increase in hardness may be attributed to the increased formation of TiB which is hard and brittle and decreases in porosity level.

Figure 4.17 depicts the microstructure and mapping of composites examined under SEM and EPMA. The presence of light and dark grey phases and some white phases are noted in all micrographs. The dark grey parts belong to the TiB phase, whereas the light grey portions correspond to the in-situ produced β-Ti, as shown in Fig. 4.17. The FeTi is shown by the arrow on the SEM images (white phase). One may observe that the size of the dark grey patches decreases and gets more refined as TiB increases as seen from micrographs presented in Fig. 4.17(a through l).

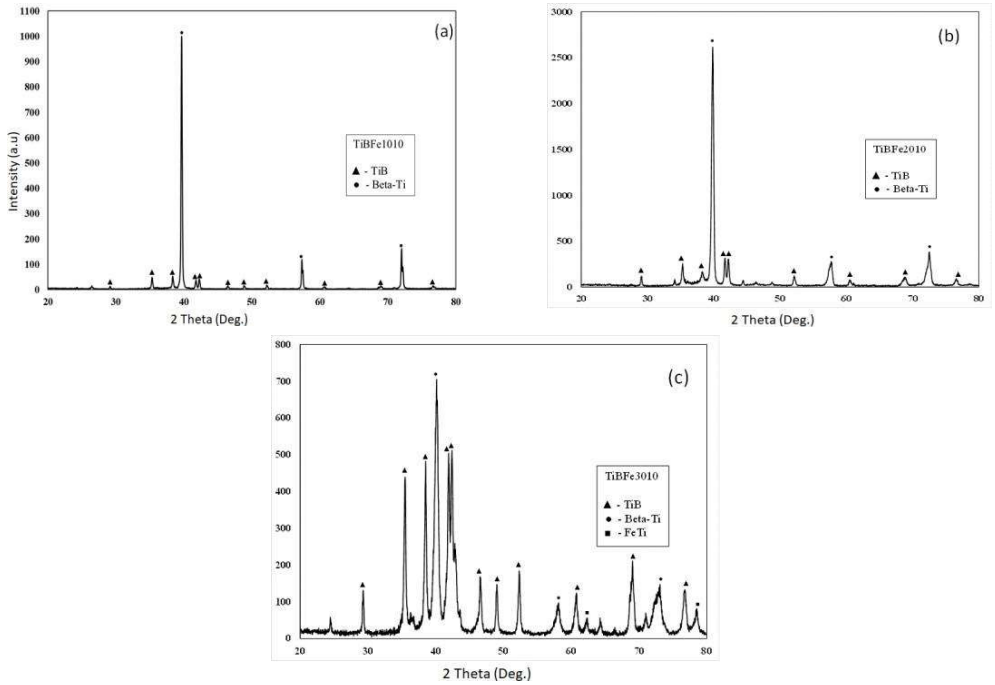

Figure 4. 16 XRD pattern of as prepared composites (a) TiBFe1010 (b) TiBFe2010 and (c) TiBFe3010

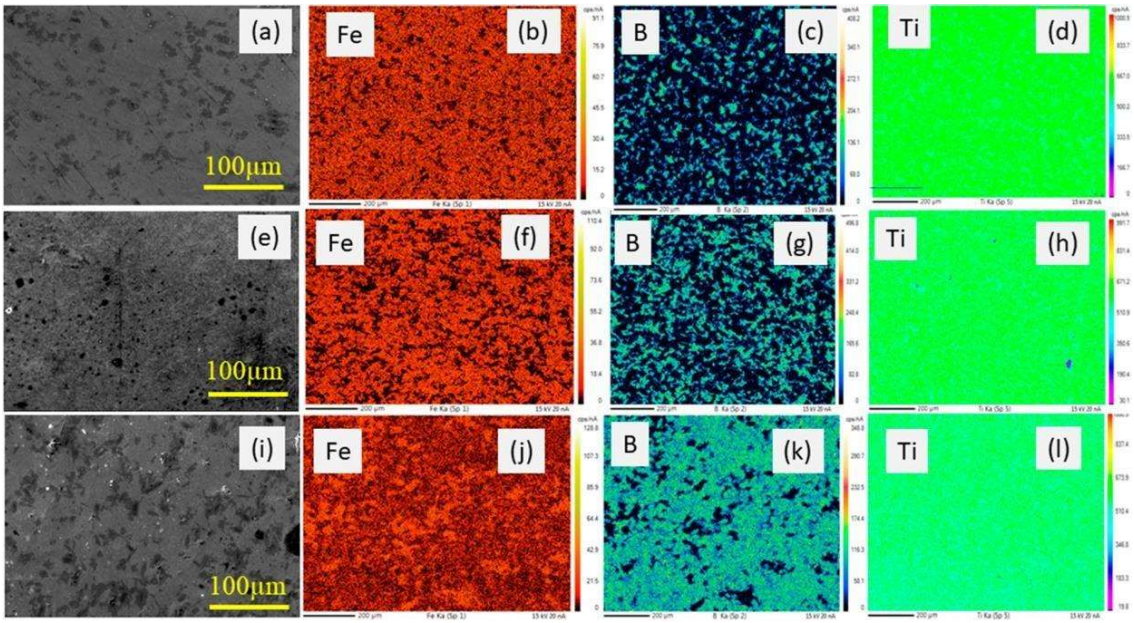

Figure 4. 17 Scanning electron micrographs showing microstructure and mapping of composites (a–d) TiBFe1010, (e–h) TiBFe2010, and (i–l) TiBFe3010, respectively

Table 4. 2 Designation, porosity, hardness, and density of composites

Designation	**Porosity**	**Hardness ($HV_{0.1}$)**	**Density (kg/m^3)**
Ti-TiB_2-10 at. % B **(TiBFe1010)**	1± 0.3%	488±11	4.84
Ti-TiB_2-20 at. % B **(TiBFe2010)**	1 ± 0.8%	718±30	4.84
Ti-TiB_2-30 at. % B **(TiBFe3010)**	1 ± 0.6%	964±22	4.90

4.3.2 FRICTION AND WEAR BEHAVIOR OF COMPOSITES

(i) Variation of coefficient of friction with time

Figure 4.18 (a through d) depicts the typical variation of coefficient of friction (COF) with time at different loads for composites i.e., TiBFe1010, TiBFe2010, and TiBFe3010. One may observe that the friction coefficient increases after the test begins and then fluctuates around a mean level before being stabilized. All the composites

have been observed to show a similar behavior at all the loads with varying amplitude of fluctuations before getting stabilized except at 10 N. However, the time taken to attain a stabilized coefficient of friction has been observed to differ depending on composition and applied load. The coefficient of friction does not appear to have stabilized even after reduction in amplitude of fluctuations after about 200 s of running. Both TiBFe2010 and TiBFe3010 are found to achieve a stable coefficient of friction after 400 s while TiBFe1010 attained the same after 500 s. At 20 N load, TiBFe2010 show a higher fluctuation before stabilizing i.e. after (approx.) 400 s while TiBFe1010 and TiBFe1030 stabilize after 200 s. At 25 N the variation of friction coefficient is relatively smooth for all the composites with marginal fluctuations after getting stabilized.

(ii) Variation of average coefficient of friction with load and composition

The variation of average COF with load is shown in Fig. 4.19 (a) whereas Fig. 4.19 (b) depicts the COF variation with composition at various loads. The average coefficient of friction has been observed to increase with increasing load from 10 to 25 N for TiBFe1010 whereas for TiBFe2010 the same has been found to increase with increase in load from 10 to 20 N beyond which it remains same. The average COF for TiBFe3010 has been found to increase with increase in load from 10 to 15 N followed by a slight decrease till 25 N. The average COF is found to decrease sharply with an increase in the content of B from 10 to 20 % which is followed by a slight decrease till 30 % of B, at all the loads. However, the decrease is relatively sharp at relatively higher loads of 20 and 25 N as seen from Fig.4.19 (b).

(iii) Variation of wear rate with normal load and Composition

Figures 4.20 (a) and (b) show the variation in wear rate with load, and composition. The wear rate of TiBFe1010 is found to decrease sharply as the load is raised from 10 to 15 N which is flowed by a further decrease till 25 N. The wear rate for both TiBFe2010 and TiBFe3010 has also been observed to decrease with increasing load but the rate of decrease quite less. The composite TiBFe1010 has the highest wear rate whereas the lowest wear rate is shown by TiBFe3010 at all loads. TiBFe3010 shows the lowest wear rate. As far as the variation of wear rate with composition at a particular load is concerned, all the composites have shown a similar variation with a different rate of decrease as the B content is raised from 10 to 20 at.% as seen from Fig. 4.20 (b). However, the wear rate is observed to either remain constant or decrease marginally with a further increase in B content from 20 to 30 at.%.

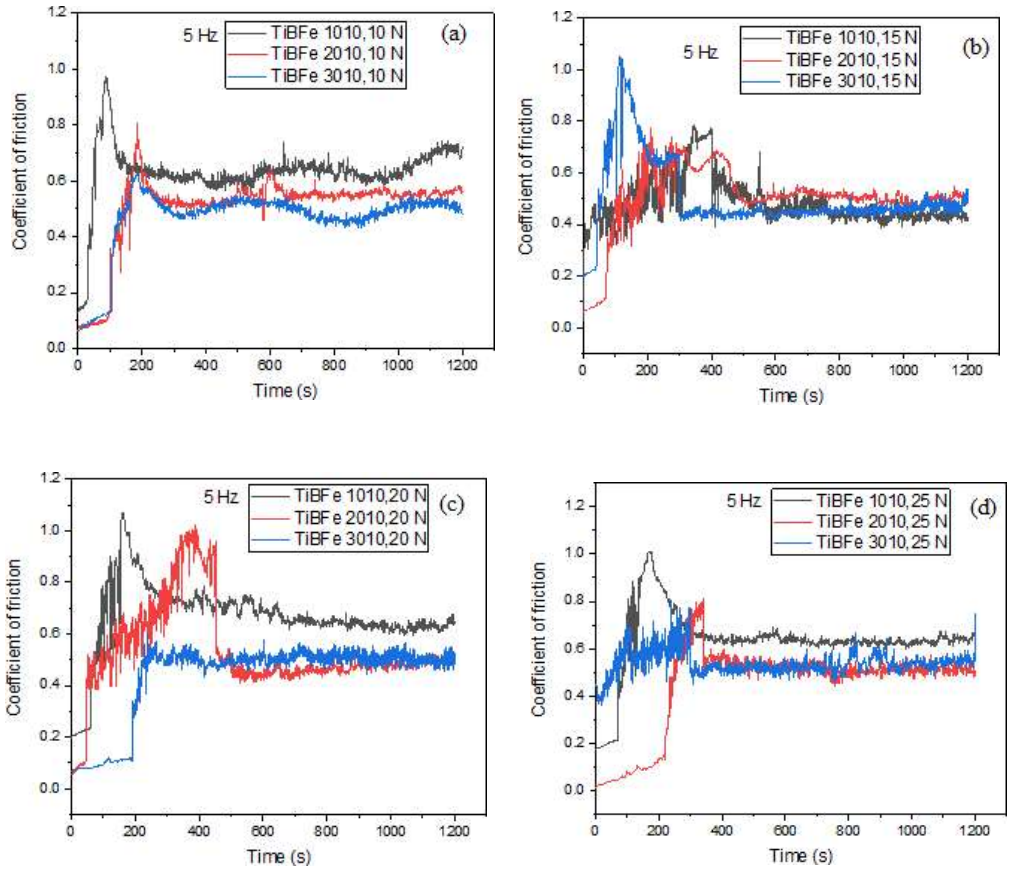

Figure 4. 18 Variation of coefficient of friction with time for TiBFe1010, TiBFe2010 and TiBFe3010 composite at different loads (a) 10 N, (b) 15 N, (c)20 N and (d) 25 N

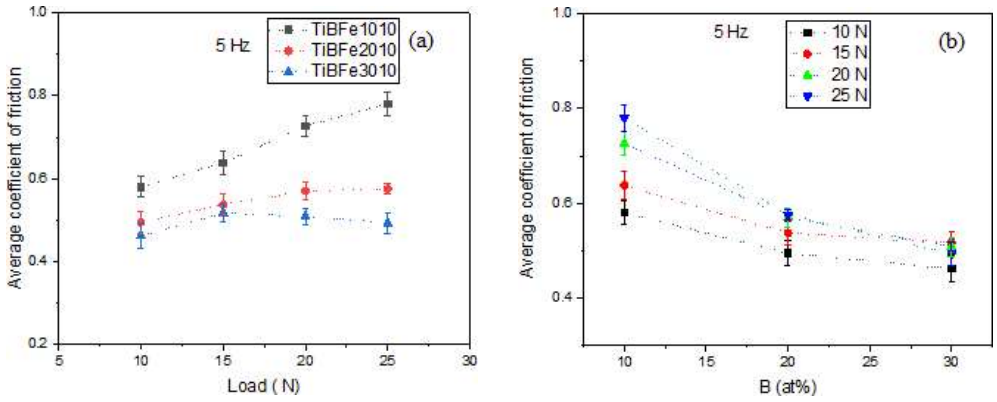

Figure 4. 19 Variation of average coefficient of friction with (a) load and (b) Composition

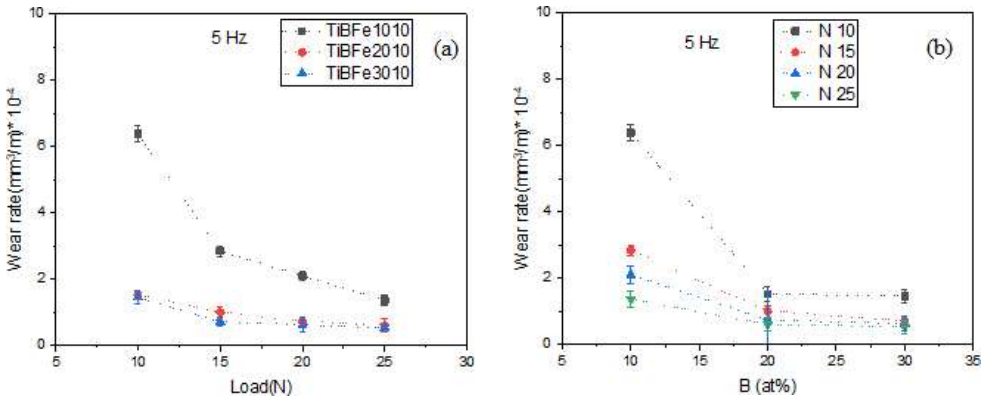

Figure 4. 20 Variation of wear rate with (a) load and (b) Composition

4.3.3 Examination of Worn Surface of Composites

Figures 4.21, 4.22, 4.23 and 4.24 present SEM micrographs of worn surfaces of TiBFe1010, TiBFe2010, and TiBFe3010 after sliding at the loads of 10, 15, 20, and 25 N, respectively. Figures 4.21 (a, c, and d) show the worn surfaces of TiBFe1010, TiBFe2010, and TiBFe3010 composites, at the lowest load of 10 N. Based on surface morphologies, various sliding marks run parallel to sliding directions with different

compaction levels of the transfer layer of wear debris. Some detachment is observed in images due to cracking, as indicated by arrows along with cracks and grooves. Loose debris may also be seen over the sliding surface. In TiBFe2010 and TiBFe3010, the transfer layer appears to be relatively compact than TiBFe1010, which helps in avoiding the metal to metal contact at interface. The elemental mapping shows presence of oxygen, pointing toward the oxidation of the worn surface and materials transferred from the counterbody on the worn surface. One may also observe the presence of cracks and delamination of the transfer layer on the micrographs TiBFe1010 and TiBFe2010, which might cause relatively higher wear than that observed for TiBFe3010, as seen from a comparison of Figs. 4.21(a, c, and d). At a load of 15 N, the worn surface of composites TiBFe1010 and TiBFe2010 is found to be covered with a compacted transfer layer as seen from Figs. 4.22 (a and b). However, the area covered by the transfer layer appears to be more in TiBFe2010 than TiBFe1010. The worn surface of TiB3010 shows the presence of small wear particles along with the compacted transfer layer at 15 N as seen from Fig. 4.22 (c).

Figure 4.23 (a through c) show the worn surface of morphology of composites at a load of 20 N. The worn surface of TiBFe1010 given in Fig. 4.23(a) shows the presence of transfer layer along with ploughing and delamination which can be seen in the inset image, whereas the micrograph of worn surface of TiBFe2010 reveals the presence of a large plate like debris on the worn surface which might have been flaked off from the transfer layer and some signs of delamination and ploughing mark as seen from Fig. 4.23 (b). The worn surface of TiBFe3010 (Fig.4.23 (c)) shows a compacted transfer layer covering a relatively larger area of the surface along with some cracks from where the transfer layer might have been delaminated.

Figure 4.24 (a through c) depicts the morphologies of composite surfaces after sliding at a load of 25 N. Figure 4.24 (a) shows deeper grooves at a few locations from

where the transfer layer appears to have got delaminated along with plate like debris on the worn surfaces of TiBFe1010, whereas a loose transfer layer along with large particles of debris and delamination features can be observed on the worn surfaces of the TiBFe2010 as seen from in Fig. 4.24 (b). Figure 4.24 (c) illustrates the presence of a scattered transfer layer on the worn surface of TiBFe3010 and a few locations of delamination.

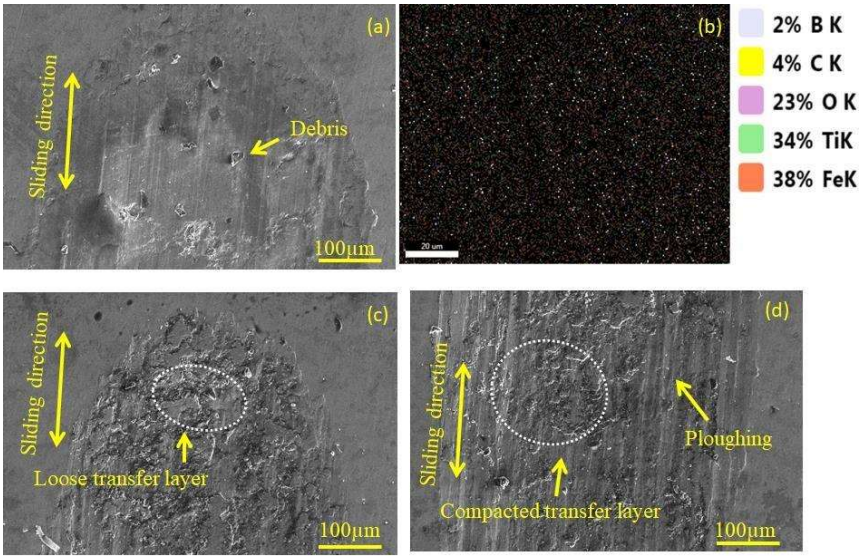

Figure 4. 21 SEM images of worn surfaces of composite at a load of 10N(a) TiBFe1010 (b) TiBFe2010, and (c) TiBFe3010

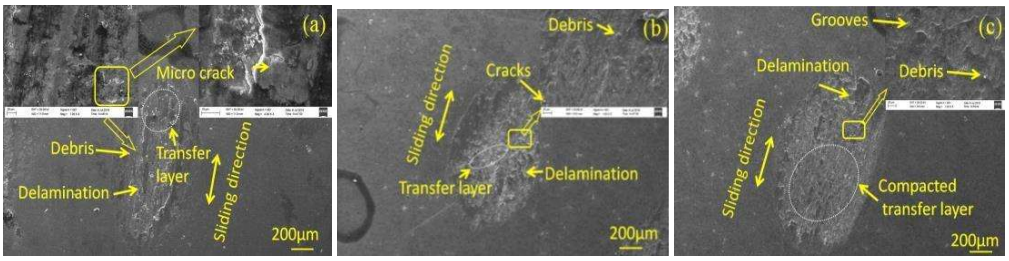

Figure 4. 22 SEM images of worn surfaces of composite at a load of 15 N

(a) TiBFe1010 (b) TiBFe2010, and (c) TiBFe3010

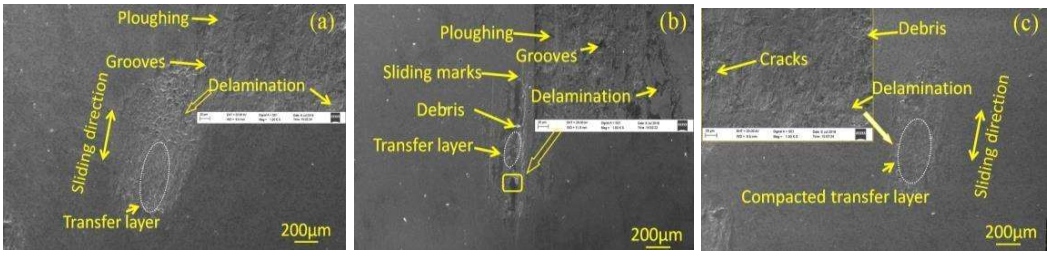

Figure 4. 23 SEM images of worn surfaces of composite at a load of 20 N
(a) TiBFe1010 (b) TiBFe2010, and (c) TiBFe3010

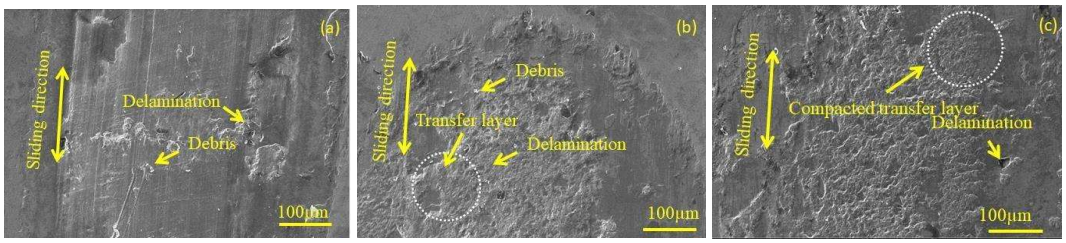

Figure 4. 24 SEM images of worn surfaces of composite at a load of 25 N
(a) TiBFe1010 (b) TiBFe2010, and (c) TiBFe3010

4.3.4 Examination of Worn Surface of Counterface

The morphologies of worn surfaces of counterface steel ball slid against TiBFe1010, TiBFe2010, and TiBFe3010 at different loads of 10, 15, 20, and 25 N are illustrated in Figs. 4.25 to 4.28 (a through c). The surface of ball worn under a load of 10 N against TiBFe1010 and given in Fig. 4.25 (a) shows presence of some abrasive marks in the direction of sliding, whereas, that slid against TiBFe2010 reveals the presence of a layer probably of material transferred from the composite with some abrasive marks in the direction of sliding as seen in Fig.4.25 (b). Figure 4.25 (c) corresponding to sliding against TiBFe3010 also presents a transfer layer containing the material transferred from the composite and their oxides as evident from EDS analysis along with some debris on the worn surface. The worn surfaces of ball slid against composites at a load of 15 N and depicted in Fig. 4.26 (a through c) also reveal presence of transfer layer with varying extent of compaction and area coverage along with some cracks. The surfaces worn at 20 N appear to be covered with a relatively loosely bound material transferred from the composite surface as seen from Fig. 4.27 (a through c). The coverage of the transfer layer is more as seen in Fig. 4.27 (c) in comparison to that in Fig. 4.27 (b) corresponding to sliding against TiBFe2010 and TiBFe3010. EDS analyses of TiBFe3010 at 10 and 20 N from Fig.4.25 (c)

and 4.27(c) shows the presence of B, Fe, Ti, and O on the counterface bearing steel ball and oxidation of the worn counterface surface. One may also observe that the increase in Ti and O content as the load is raised from 10 to 20 N, indicating the enhanced probability of oxide formation with increasing load due to increased frictional heat.

The worn surface morphologies of the steel ball slid against TiBFe1010, TiBFe2010, and TiBFe3010 composite at 25 N are presented in Fig. 4.28 (a to c). Figure 4.28 (a) corresponding to sliding against TiBFe1010 shows the presence of loosely bound transfer layers at a few places along with debris and cracks on the surface, whereas the worn surface of ball slid against TiBFe2010 and shown in Fig 4.28 (b) is covered with a compacted transfer layer along with some abrasive marks in the sliding direction. However, the worn surface given in Fig. 4.28 (c) reveals the presence of a well-compacted transfer layer containing materials from TiBFe3010 along with some fine debris particles.

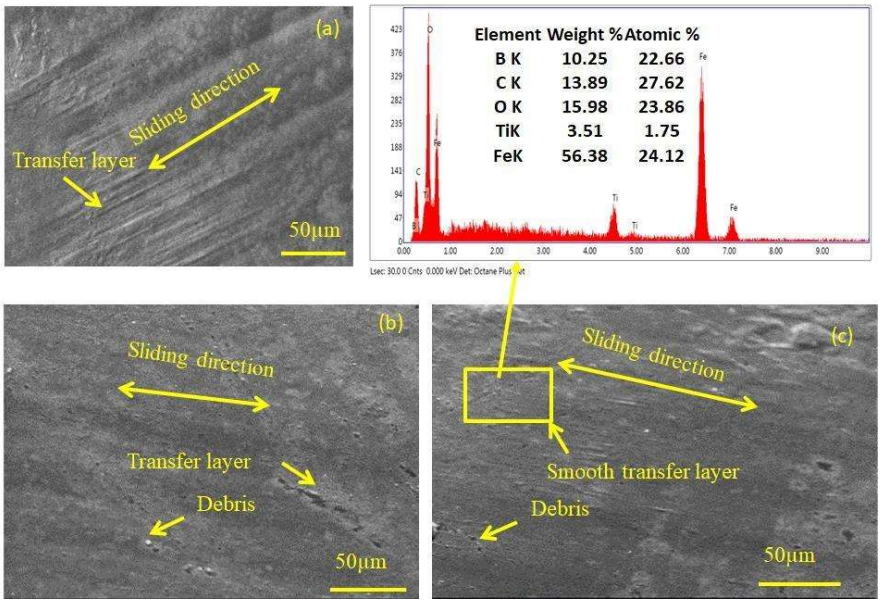

Figure 4. 25 Worn surfaces of bearing steel ball slid against (a) TiBFe1010 (b) TiBFe2010 and (c) TiBFe3010 composite at a load of 10N

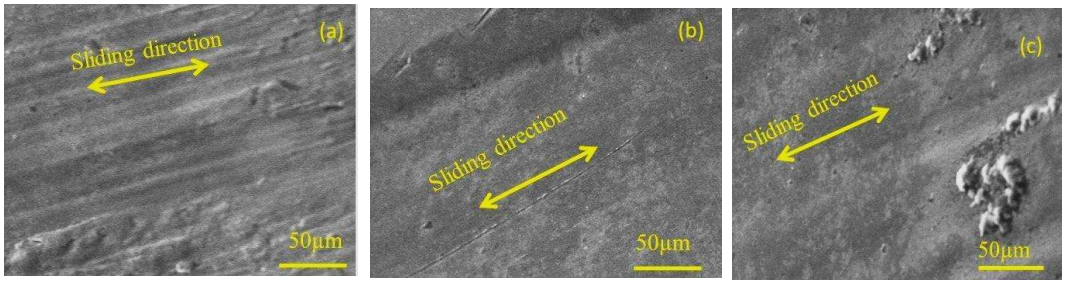

Figure 4. 26 Worn surfaces of bearing steel ball slid against (a) TiBFe1010 (b) TiBFe2010 and (c) TiBFe3010 composite at a load of 15N

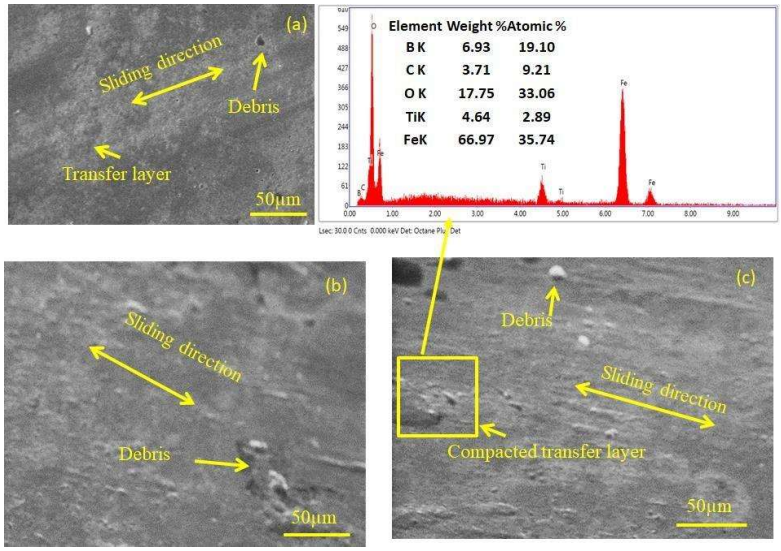

Figure 4. 27 Worn surfaces of bearing steel ball slid against (a) TiBFe1010 (b) TiBFe2010 and (c) TiBFe3010 composite at a load of 20N

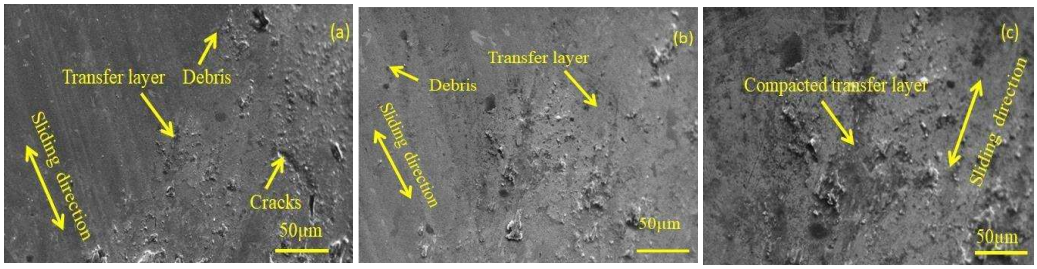

Figure 4. 28 Worn surfaces of bearing steel ball slid against (a) TiBFe1010 (b) TiBFe2010 and (c) TiBFe3010 composite at a load of 25N

4.3.5 Examination of Wear Debris

The micrographs of debris collected after sliding at a load of 10 N and illustrated in Fig. 4.29 (a, b and c) reveal the presence of some large plate like debris which might

have come from the delamination of transfer layer along with some loose wear particles of varying sizes. The debris for TiBFe1010 and TiBFe2010, collected after sliding under a load of 25 N reveal the presence of some fine and agglomerated wear particles as evident from Figs. 4.30 (a and b). However, a few compacted lumps of debris particles with signs of cracking could be seen in the micrographs of the wear debris corresponding to TiBFE3010 as seen from Fig. 4.30 (c).

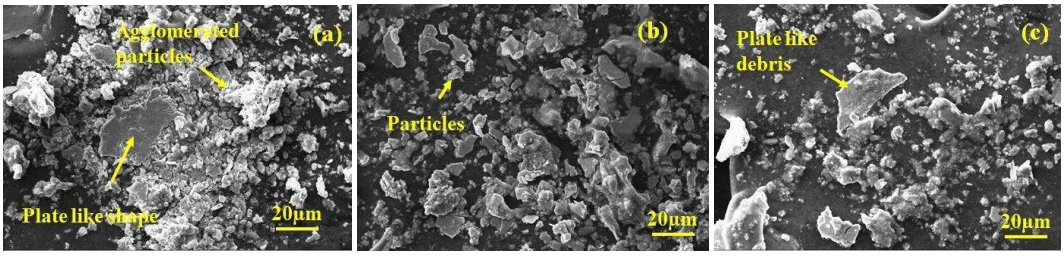

Figure 4. 29 SEM micrographs of wear debris (a) TiBFe1010 at 10N load (b) TiBFe2010 at 10N load (c) TiBFe3010 at a load of 10 N

Figure 4. 30 SEM micrographs of wear debris (a) TiBFe1010 at 25N load (b) TiBFe2010 at 25N load (c) TiBFe3010 at a load of 25 N

Figure 4.31 shows X-ray diffraction patter of the pooled wear debris which reveals the presence of TiB, TiO, Ti_2O, B_2O_3, and FeO in the debris.

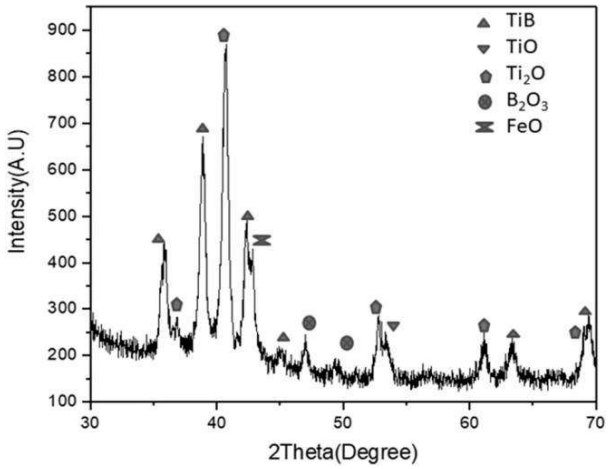

Figure 4. 31 XRD spectra of the debris

4.4 DISCUSSION

The higher coefficient of friction observed for TiBFe1010 in comparison with other composites may be ascribed to its relatively lower hardness compared to TiBFe2010 and TiBFe3010 which results in a relatively higher real area of contact. The lowest friction shown by TiBFe3010 at all the loads shown in Fig. 4.19 (a and b) may also be explained based on its highest hardness leading to a relatively lower real area of contact. However, it is well established that hardness is not only the single factor affecting the friction but other phenomena occurring during sliding like formation of debris, its oxidation, ability of to form a transfer layer over the sliding surface, the degree of compaction and extent of coverage of transfer layer on the surface, formation-detachment-reformation of transfer layer, and presence of lubricious oxide on the surface also contribute in controlling friction and wear behaviour. The surface of the composites has been observed to be covered by a transfer layer with varying degree of compaction and coverage of surface depending on the applied load. The layer is well compacted at relatively higher loads than lower ones due to increased frictional heating. As stated earlier, a substrate with a higher hardness is able to

hold a relatively thicker transfer layer before it gets detached. EDS spectrums of wear debris shown in Figs. 4.21, 4.27, reveal the presence of oxygen and whereas XRD pattern shown in Fig.4.31 reflects the presence of oxides (TiO, Ti_2O, B_2O_3, and FeO) in the wear debris. B_2O_3 has been shown to be lubricious in nature (ref). The transfer layer containing the oxidic debris is expected to provide low shearing junctions at interface which lead to lowering of the friction. A comparison of Figures 4.21(a, b, c), 4.22(a, b, c), 4.23(a, b, c), and 4.24 (a, b, c) show that the worn surface of TiBFe3010 is covered by a well compacted, smooth and relatively thicker transfer layer in comparison to TiBFe1010 and TiBFe2010. Hence, it is not surprising that the composite TiBFe3010 has the lower coefficient of friction. At a particular load, the friction coefficient has also been observed to decrease with increasing content of TiB_2, as seen from Fig. 4.19 (b), and the same may also be explained based on the presence of the transfer and its extent of coverage provided to the underlying substrate along which is helpful in reducing the metal–metal contact and, in turn, adhesion between the surfaces in contact.

The wear rate has been found to decrease with increasing load from 10 to 25 N for all the composites as seen from Fig. 4.20 (a) and TiBFe1010 has shown the highest wear rate and TiBFe3010 the lowest. A decreasing wear rate with increasing load may again be explained based on the presence of a transfer layer, its degree of compaction, smoothness and extent of area coverage as explained earlier for frictional behavior. At 10 N, the TiBFe1010 worn surface appears to be moderately torn (Fig. 4.21 a), however at 25 N (Fig. 4.24 a), it reveals the presence of a compacted transfer layer that is observed to have detached at several locations. This might have resulted in more material loss and, thus, high wear in TiBFe1010. However, at both 10 N and 25 N, a smooth transfer layer is seen on the surfaces of both TiBFe2010 and TiBFe3010 as seen from Figs. 4.21 (b and c) and 4.24 (b and c). However, some delamination is observed at the worn surface of TiBFe2010 at

10 N. In contrast, it is discovered that there are deep grooves present at 25 N that run parallel to the direction of sliding, suggesting that this material may have worn out more quickly than TiBFe2010. The presence of grooves may be ascribed to the abrasive action of hard TiB and the presence of TiB in wear debris is confirmed by XRD shown in Fig. 4.31. The increasing amount of TiB appears to be detrimental to the friction and wear properties if it is as a loose wear debri particle and fail to get embedded and compacted into the form of transfer layer, despite improving the hardness due to its inherent brittleness. The current investigation demonstrates that, under the conditions of lad and frequency used in the present study, TiBFe3010 has shown the optimum tribological performance in term of both the coefficient of friction and the wear rate.

Based on the results and discussion presented above, it can be inferred that TiTiBFe composites can be successfully synthesized through an in-situ reaction between Ti and TiB_2 consisting of a fixed content of Fe, i.e., 10%, and varying amount of TiB_2. TiBFe3010 showed the lowest coefficient of friction and wear rate due to the dominating effect of the transfer layer, its area coverage and presence of lubricious oxides. The dominating mechanisms of wear have been found to be ploughing, abrasion, oxidation, and delamination.